Catalysis Today 154 (2010) 210–216

Contents lists available at ScienceDirect

Catalysis Today

journal homepage: www.elsevier.com/locate/cattod

Reducing the deactivation of Ni-metal during the catalytic partial oxidation of a surrogate diesel fuel mixture

Daniel J. Haynes[a,b,*], Andrew Campos[c,1], Mark W. Smith[d,2], David A. Berry[a,3], Dushyant Shekhawat[a,4], James J. Spivey[c,5]

[a] U.S. Department of Energy, National Energy Technology Laboratory, 3610 Collins Ferry Road, Morgantown, WV 26507, United States
[b] URS-Washington Division, 3604 Collins Ferry Road, Suite 200, Morgantown, WV 26505, United States
[c] Louisiana State University, Department of Chemical Engineering, 110 South Stadium Drive, Baton Rouge, LA 70803, United States
[d] REM Engineering Services, 3566 Collins Ferry Road, Morgantown, WV 26505, United States

ARTICLE INFO

Article history:
Available online 7 May 2010

Keywords:
Pyrochlore
Hexaaluminate
Nickel
Logistic fuel reforming
Partial oxidation catalyst

ABSTRACT

Ni catalysts are active and selective for the conversion of hydrocarbon into synthesis gas. However, conventional supported Ni catalysts rapidly deactivate at the high temperatures required for partial oxidation of diesel fuel by sintering and metal vaporization, as well as by carbon deposition and sulfur poisoning. Thus, to reduce deactivation Ni (3 wt%) was substituted into the structures of Ba-hexaaluminate (BNHA) and La–Sr–Zr pyrochlore (LSZN), and their activity was compared to a supported Ni/Al_2O_3 for the catalytic partial oxidation (CPOX) of a surrogate diesel fuel. Characterization by XRD showed a single phase β-alumina for the hexaaluminate, while LSZN had a pyrochlore structure with a defect $SrZrO_3$ perovskite phase. Temperature programmed reduction experiments confirmed Ni was reducible in all catalysts. XANES results confirmed that Ni atoms were substituted into the hexaaluminate and pyrochlore structures, as spectra for each catalyst showed different coordination environments for Ni compared to a NiO standard. During CPOX activity tests (T = 900 °C and WHSV = 50,000 scc/g_{cat}/h), the LSZN pyrochlore produced stable H_2 and CO yields in the presence of 5 wt% 1-methylnaphthalene and 50 ppmw dibenzothiophene/n-tetradecane for 2 h, while both Ni/Al_2O_3 and BNHA catalysts were irreversibly deactivated by this mixture over the same time. Activity loss was strongly linked to carbon formation.

1. Introduction

The chemical energy from fossil fuels can be harnessed in a more efficient and environmentally friendly manner by the catalytic reforming the fuel into synthesis gas for use in fuel cells rather than combustion. This would help to extend the life of fossil fuel reserves until renewable and sustainable sources like solar, wind, and biomass become more competitive. In addition, harmful greenhouse gas emissions associated with their combustion are minimized. Of available fuel cells, solid oxide fuel cells (SOFCs) have shown to be a promising technology. Their high operating temperature (800 °C) allows for less stringent fuel requirements, which makes them appealing for a broad range of applications. Some of these applications, for example auxiliary power units (APUs) for diesel trucks and military uses, will rely on diesel as the fuel source. Conversion of diesel fuel into a H_2-rich synthesis gas suitable for SOFCs can be done by three main chemical routes: steam reforming, catalytic partial oxidation (CPOX), or autothermal reforming. CPOX reforming units are attractive for these applications because they are light weight and less complicated compared to those designed for the other reforming modes.

Ni is known to be an active and selective catalyst for the CPOX of various hydrocarbon fuels into synthesis gas [1–9]. Further, its cost and availability make it desirable for commercial use. Choosing Ni as a catalyst to reform diesel, however, has serious drawbacks that need to be overcome before a commercially viable catalyst can be developed. As in all reforming reactions, carbon formation inevitably occurs as an undesired side reaction, usually leading to catalyst deactivation and eventual reactor plugging [10,11]. Difficulties with carbon accumulation become more significant during

* Corresponding author at: U.S. Department of Energy, National Energy Technology Laboratory, 3610 Collins Ferry Road, Morgantown, WV 26507, United States. Tel.: +1 304 285 1355; fax: +1 304 285 0903.
E-mail addresses: Daniel.Haynes@ur.netl.doe.gov, daniel.haynes@pp.netl.doe.gov (D.J. Haynes), Acampo2@lsu.edu (A. Campos), Mark.Smith@re.netl.doe.gov (M.W. Smith), David.Berry@netl.doe.gov (D.A. Berry), Dushyant.Shekhawat@netl.doe.gov (D. Shekhawat), jjspivey@lsu.edu (J.J. Spivey).
[1] Tel.: +1 225 578 7032.
[2] Tel.: +1 304 285 4126.
[3] Tel.: +1 304 285 4430.
[4] Tel.: +1 304 285 4634.
[5] Tel.: +1 225 578 3690.

0920-5861/$ – see front matter © 2010 Elsevier B.V. All rights reserved.
doi:10.1016/j.cattod.2010.03.072

the reforming of diesel, due to the large amount of carbon forming precursors present. Using Ni catalysts compounds this problem even further as one of the main issues associated with using Ni being the inability to limit the rate of carbon formation [6,12].

During reforming the morphology of the carbon species formed on Ni catalysts can have three main forms: encapsulating, pyrolytic, and/or filamentous [13]. In particular, filamentous or whisker carbon is known to be promoted specifically by traditional supported Ni catalysts because carbon atoms are soluble in Ni crystals [13–15]. Filament carbon cannot form on most other catalysts, such as group VIII metals, as they do not dissolve carbon. The growth of carbon filaments is believed to occur as adsorbed carbon atoms diffuse through large Ni crystallites (>7 nm [6]) and condense at the base, thus lifting the Ni particle off the surface and forming the whisker [13,15]. Although Ni remains active during this process, continual whisker growth eventually degrades the catalyst particles and leads to reactor plugging [15].

Carbon formation is not the only issue that adversely affects catalytic activity of Ni during the reforming of diesel. Another concern is sulfur poisoning. Although the sulfur content in commercial diesel fuel has recently been regulated to lower levels (~15 ppm) [16], other fuels, like JP8, can have much higher levels (between 300 and 3000 ppm) [17]. Sulfur poisoning likely occurs through the reaction of sulfur-containing compounds with metallic Ni particles, forming inactive surface Ni-sulfide species [18].

The deactivation by carbon and sulfur may, however, be controlled by the substitution of Ni into the structure of a refractory metal oxide. Carbon formation and sulfur poisoning are known to be more significant on larger metallic clusters, and require a minimum number of Ni atoms to take place [4]. Dispersing Ni in a thermally stable structure would avoid the critical ensemble size of Ni atoms that lead to deactivation by carbon deposition or sulfur poisoning. In addition, as the metal is bound within the structure of the oxide lattice, problems associated with the use of traditional supported catalysts at elevated temperatures would be reduced, including metal vaporization as well as the sintering of Ni crystallites into larger clusters that are easily poisoned [13,19].

Previously [4,20–22], two refractory oxides, Ba–Ni-hexaaluminate (BNHA) and La–Sr–Zr–M (LSZM; M = Rh or Ru) pyrochlore, have shown the thermal and chemical stability needed for CPOX. The BNHA catalyst (3 wt% Ni) was able to produce equilibrium yields during 5 h CPOX of n-tetradecane at 850 °C and WHSV = 50,000 scc/g_{cat}/h, but is untested in the presence of contaminants commonly found in diesel. Meanwhile, a La–Sr–Zr pyrochlore substituted with either Rh or Ru has been shown to improve reforming properties of these metals in the presence of contaminants compared to conventional Rh or Ru supported metal catalysts [20,21]. The same La–Sr–Zr formulation substituted with Ni (3 wt%), may also be able to enhance the reforming properties of Ni and avoid deactivation.

The objective of the present work is to evaluate Ba–Ni-hexaaluminate (BNHA), and La–Sr–Zr–Ni (LSZN) (both containing 3 wt% Ni) as catalysts for the CPOX of a contaminant laden surrogate diesel fuel mixture containing both polyaromatic, and organosulfur compounds. A conventional supported 3.0 wt% Ni/Al_2O_3 will also be tested for comparison.

2. Experimental

2.1. Catalyst preparation

A variation of the Pechini method [23] and the co-precipitation method [4] were used to prepare the 3 wt% Ni-containing pyrochlore and hexaaluminate catalysts, respectively. Nominal formulas for these oxide catalysts are shown in Table 1. The supported 3 wt% Ni/Al_2O_3 catalyst was prepared by an incipient wetness technique in which γ-Al_2O_3 powder was impregnated with $Ni(NO_3)_2$ solution to give a 3 wt% Ni loading. The catalyst was then calcined at 950 °C, for 4 h.

Table 1
Theoretical compositions for mixed oxide catalysts.

Pyrochlore	Hexaaluminate
$La_{1.50}Sr_{0.50}Zr_{1.72}Ni_{0.28}O_{7-\delta}$	$BaNi_{0.4}Al_{11.6}O_{18.8}$

Table 2
Scanning parameters for Ni XANES.

Element (edge keV)	Ni (8.333)
Scan interval (eV, rel. edge)	−150, −20, 40, 100, 200
Step size (eV)	5,0.3,1.0,2.0
Integration time (s)	5

2.2. Characterization

A PanAnalytical X'pert Pro X-Ray unit (Model No. PW 3040 Pro) was used for X-ray diffraction analysis of the powders. Subsequent peak identification of the X-ray data was performed using X'pert High Score Plus software, version 2.1. Temperature programmed reduction (TPR) experiments were performed in a Micromeritics Autochem 2910 unit. Experimental details for the TPR experiments have been specified in a previous study [22]. K-edge X-ray Absorption Near Edge Structure (XANES) spectra of the Ni-containing pyrochlore and hexaaluminate catalysts were taken at the DCM beamline at LSU's synchrotron facility, the J. Bennett Johnston Sr. Center for Advanced Microstructures and Devices (CAMD, Baton Rouge, LA). The operating energy of CAMD is 1.3 GeV, with a typical ring current between 100 and 200 mA. The DCM beamline was operated with Ge(2 2 0) crystals in the monochromator, and has an approximate resolution of 2.0 eV at the energy range in this study. A γ-Ni foil (6 μm thick) spectrum was collected during each scan to maintain energy calibration between runs. NiO (99.998% metals basis, Alfa Aesar) was used to compare with the spectra of the catalysts. The samples were placed on Kapton® tape and scanned in fluorescence mode using a Vortex™ Si drifts detector (50 mm^2 active area) under ambient conditions with the scanning parameters given in Table 2. The standards were scanned in transmission mode with a 1 s integration time.

2.3. Experimental setup

A detailed description of the reactor system has been documented elsewhere [24]. Catalytic testing was performed in a fixed-bed continuous-flow reactor (Autoclave Engineers, Model no. BTRS Jr). The catalyst was loaded into an 8 mm i.d. tubular reactor and diluted with quartz sand of the same particle size as the catalyst, to minimize temperature gradients and channeling throughout the bed. Heat was supplied via a split-tube furnace, and the bed temperature was measured by an axially centered thermocouple. External heating was required to ensure a uniform temperature distribution throughout the catalyst bed. Although the CPOX reaction is highly exothermic, the reactant flow rates were too low for the reaction to sustain itself because of significant heat losses.

2.4. Experimental conditions

n-Tetradecane (TD), 1-methylnaphthalene (MN) and dibenzothiophene (DBT) were used to represent the major paraffin, aromatic, and sulfur compounds, respectively, that are commonly found in diesel fuels [25]. Fresh catalyst powders used in reaction studies

Table 3
Reaction conditions for CPOX experiments.

Reaction conditions	
O/C ratio	1.2
GHSV (scc/g_{cat}/h)	50,000
Pre-heat (°C)	375
Bed temperature (°C)	900
Catalyst bed (mg)	480
Pressure (MPa)	0.23

consisted of the oxide form of the respective catalyst, no H_2 pre-treatment was performed. The experimental procedure involved three steps. First, the CPOX of TD only was conducted for 1 h to establish baseline activity and selectivity of the catalyst. Next, the feed was switched to 5 wt% MN and 50 ppmw DBT in TD for 2 h. Finally, the feed was switched back to TD only for 1 h to examine activity recovery. Experimental conditions are detailed in Table 3. After CPOX experiments a temperature programmed oxidation (TPO) was performed to determine the amount of carbon deposited on the catalyst after reaction. The carbon was oxidized by passing a 10% mixture of O_2/N_2 over the catalyst while being heated from 200 °C to 900 °C at 1 °C/min. The TPO results reported here include carbon deposited on the quartz as well as on the catalyst. Previous TPO results after CPOX of TD only in this same reactor containing quartz only show that significant carbon is deposited on the quartz, and can actually be greater than that formed in a directly comparable experiment in a reactor containing quartz and an active catalyst, showing that carbon deposition on the quartz and catalyst are not independent processes [22]. However, the deactivation observed on the catalyst/quartz bed in this earlier study, as measured by H_2/CO yield, differs significantly from that for quartz only, indicating that the TPO results can provide at least qualitative comparisons of carbon deposition among the catalysts reported here.

The dry gas products H_2, CO, CO_2, and N_2 were analyzed continuously by an online Thermo Onix mass spectrometer (Model no. Prima δb, a 200 a.m.u. scanning magnetic sector), while gaseous hydrocarbon products (C_1–C_6) were analyzed with an HP5890 gas chromatograph equipped with a flame ionization detector. Five GC samples were taken over the course of a 4 h experiment: the first at the beginning of the experiment (~after 5 min), then one per h as the experiment progressed. Carbon balances (as measured by GC and MS) during runs for all experiments were 100 ± 10%. Steam concentration was not measured analytically; however, it was estimated indirectly from mass balance calculations of hydrogen- and oxygen-containing species in the product stream.

The following Eqs. (1)–(3) were used in the analysis of the experimental data. The yield of each dry gas product, i.e. H_2, CO, CO_2, and CH_4 was calculated by Eq. (1).

$$\text{Yield of A}\,(\%) = \frac{\text{Moles of A produced} \times 100}{N \times \text{moles of TD fed to the reactor}} \quad (1)$$

where N is the number of moles of H_2 per mole of hydrocarbon for H_2 yields and is the number of moles of carbon in the hydrocarbon fuel for yields of carbon containing products.

Hydrocarbon (HC) yields were determined using Eq. (2).

$$\text{HC yield}\,(\%) = \frac{\text{Moles of HC produced} \times i \times 100}{N \times \text{moles of TD fed to the reactor}} \quad (2)$$

where i is the number of moles of carbon per mole of hydrocarbon in the product (i.e. i would be 2 for ethane) and N is the number of moles of carbon in the hydrocarbon fuel.

A carbon balance was determined by Eq. (3).

$$\text{Carbon balance}\,(\%) = \frac{(\text{CO} + \text{CO}_2 + \sum_i^{i=1-6} i\text{C}_i\text{H}_r) \times 100}{N \times \text{moles of TD fed to the reactor}} \quad (3)$$

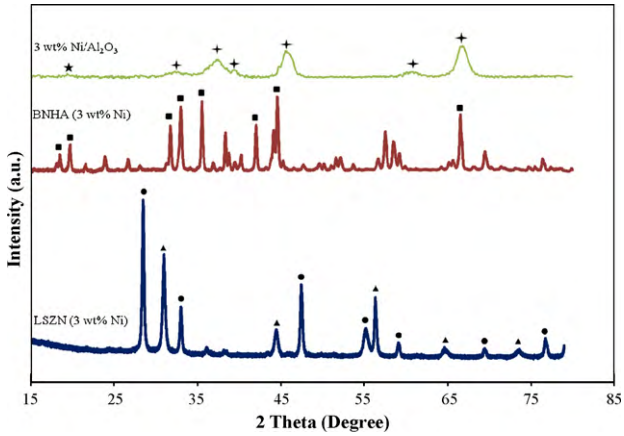

Fig. 1. XRD profiles for fresh LSZN (3.0 wt% Ni), BNHA (3.0 wt% Ni), and 3 wt% Ni/Al_2O_3, catalysts. Peaks from $La_2Zr_2O_7$ pyrochlore (●); peaks from $SrZrO_3$ perovskite (▲); main peaks for $BaAl_{12}O_{19}$ (■); main peaks for alumina oxide (✦) (PDF: 00-004-0875); peak for monoclinic alumina, q-Al_2O_3 (PDF: 00-035-0121) (⋆).

where i is the number of moles of carbon per mole of hydrocarbon in the product (i.e. i would be 2 for ethane), N is the number of moles of carbon in the hydrocarbon fuel and r is the number of hydrogen atoms contained in the hydrocarbon product.

3. Results

3.1. XRD

XRD profiles for LSZN, BNHA, and Ni/Al_2O_3 catalysts are presented in Fig. 1. The reflection pattern for LSZN confirms that the pyrochlore phase is achieved, but is also accompanied by a defect $SrZrO_3$ perovskite. The presence of $SrZrO_3$ is consistent with pyrochlore catalysts containing La, Sr, and Zr (with either Rh or Ru) used in previous studies [21,22], and is due to the low solubility (~2.5 mol%) of Sr in the $La_2Zr_2O_7$ structure [26]. The pattern of BNHA shows peaks characteristic of single phase $BaAl_{12}O_{19}$. The XRD scan of 3 wt% Ni/Al_2O_3 reveals peak intensities which correspond primarily to a form alumina oxide with the diffraction pattern reference code PDF: 00-004-0875 in the inorganic crystal structure database (ICSD), indicating the calcination treatment (950 °C for 4 h) has transformed the Al from the ions from the cubic γ-Al_2O_3 into a spinel-like configuration. However, the low angle peak at 19.2° has lost intensity, suggesting some Al ions are beginning to occupy a monoclinic arrangement (PDF: 00-035-0121). In addition to the various phases of alumina, a $NiAl_2O_4$ spinel phase can also form when Ni–Al_2O_3 systems are calcined at temperatures above 550 °C [27]. This catalyst was treated at 950 °C, which would suggest that the formation of this phase is likely. However, the XRD was not able to detect whether the formation of the $NiAl_2O_4$ spinel has occurred. This could possibly be explained by the fact that at a 3 wt% Ni loading, the main peak for $NiAl_2O_4$ (37°) is not intense enough to be observed, especially when it is overlapped by a relatively intense peak for the alumina oxide that is present in much greater abundance.

3.2. H_2-temperature programmed reduction

TPR experiments were performed to examine the reduction properties of Ni in each material (Fig. 2). As expected, a large portion of the Ni is reducible on the Ni/Al_2O_3 catalyst. Two peaks are observed during reduction for 3 wt% Ni/Al_2O_3: a smaller shoulder at 700 °C and, a large broad peak at 880 °C. The temperatures observed here are higher than temperatures at which reduction of bulk NiO → Ni° normally occurs (450–500 °C) [28]. The increase

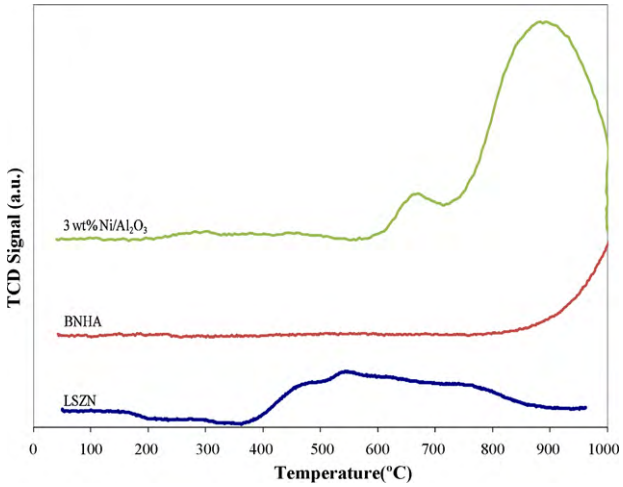

Fig. 2. H_2-TPR curves for 3 wt% Ni/Al_2O_3, BNHA (3.0 wt% Ni), and LSZN (3.0 wt% Ni).

in reduction temperatures suggests a stronger interaction between the Ni and Al species on the catalyst, which is caused by the high calcination temperature used for this catalyst-950 °C for 4 h. A profile similar to that obtained in this study has been observed previously for a 3 wt% Ni/Al_2O_3 catalyst calcined at 650 °C, and was attributed to the presence of the $NiAl_2O_4$ spinel phase [27]. Given the similarity in reduction temperatures used by Ibrahim et al. [27], and that of this study, the large reduction peak at 880 °C shows that a majority of Ni in the catalyst of this study also resides in the $NiAl_2O_4$ phase despite not being detected by XRD analysis (Fig. 1). A low temperature peak is also observed at about 685 °C. This peak is also much higher than the reduction of bulk Ni, but lower than the reduction of $NiAl_2O_4$, indicating there are Ni-oxide species having a strong interaction with the Al_2O_3 support, but they are not completely incorporated into the spinel structure [27].

The TPR profile for BNHA shows that Ni substituted into the hexaaluminate structure does not become reducible until rather high temperatures. Reduction begins at roughly 850 °C, and increases until the temperature limit of the furnace is reached. The refractory nature of the Ni-oxide species in the hexaaluminate lattice is a result of a strong interaction between the Ni and the surrounding atoms in the hexaaluminate structure [29,30]. A complete reduction curve recorded by Chu et al. [29] for a BNHA catalyst with similar composition, $BaNi_{0.3}Al_{11.7}O_{19}$, shows that reduction continues up to 1200 °C, with two distinct peaks observed at 950 °C and 1100 °C. Each peak corresponds to the reduction of Ni in a different part of the structure. The first peak is likely due to the reduction of Ni atoms that occupy an Al-interstitial site near the mirror plane [31]. Oxygen in this region is less tightly bound than oxygen in the spinel block [4], and is easily accessible by H_2 diffusing through the lattice [31]. The second reduction peak can then be attributed to the reduction of Ni positioned inside the spinel block. Higher temperatures are needed to reduce the Ni in this coordination because the atoms are more tightly packed, and therefore shielded from reduction [31]. The temperature range for the reduction of the BNHA catalyst (Fig. 2) is consistent with the low temperature peak seen by Chu et al. [29], suggesting this can likely be attributed to reduction of interstitial Ni atoms. However, reduction appears to be shifted to a higher temperature for the BNHA in Fig. 2 probably because of differences in material preparations and calcination temperatures.

Reduction of Ni in the pyrochlore structure is not as obvious as the other two catalysts. At first glance it appears that the reduction of Ni occurs over the temperature range corresponding to the reduction of bulk NiO. However, reduction of the pyrochlore seen in Fig. 2, which begins around 400 °C, is actually the reduction of oxygen from the bulk $La_2Zr_2O_7$ structure [21,22]. Comparing the TPR curve for LSZN to a TPR curve for $La_2Zr_2O_7$ (LZ) [22], and another for $La_{1.5}Sr_{0.5}Zr_{1.95}\ Ru_{0.05}O_{7-\delta}$ (LSZRu) [21] shows similarly shaped curves from 400 °C up to about 650 °C, regardless of whether an active metal is substituted into the structure or not. After 650 °C, reduction curves for the LZ and LSZRu materials return to baseline, while reduction continues for the LSZN catalyst up to about 900 °C. This behavior reveals that a portion of accessible Ni in the pyrochlore structure is reducible over an intermediate temperature range between that of the $NiAl_2O_4$ spinel of the supported catalyst and that of the Ni-substituted hexaaluminate (BNHA).

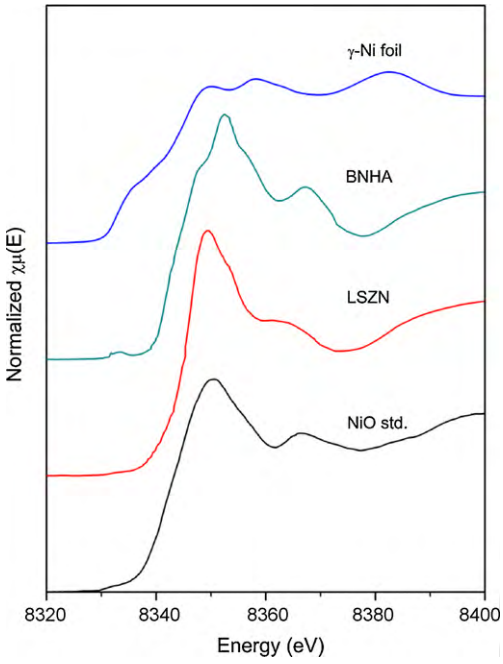

Fig. 3. XANES spectra for fresh BNHA and LSZN catalysts compared to NiO and γ-Ni foil standards.

3.3. XANES

A comparison between the XANES spectra of the BNHA and LSZN catalysts with the Ni standards is shown in Fig. 3. The pre-edge feature observed in the LSZN, BNHA, and NiO standard spectra is located at 8333 eV, which is due to $1s \rightarrow 3d$ transitions, and is indicative of an oxide-type phase.

The spectra of the BNHA and LSZN catalysts confirm that Ni is primarily in the 2+ oxidation state [32–34]. However, significant differences between the NiO standard and the spectra of the BNHA and LSZN catalysts indicate different local coordination environments for the catalysts relative to NiO, as expected.

Farges et al. [35] studied the pre-edge feature of Ni^{2+}-containing species and found information about the coordination environment of Ni based on the shape and location of the pre-edge feature. The BNHA catalyst has a sharper pre-edge feature relative to the 6-coordinated NiO. This is indicative of Ni being either 4 or 5-coordinated, on average [35]. The LSZN catalyst has a weaker pre-edge feature that is similar to the NiO which indicates that it is on average 6-coordinated.

3.4. CPOX reaction studies

3.4.1. Equilibrium and blank reactor

Table 4 shows equilibrium and blank reactor (quartz sand) product yields at conditions of interest here. High H_2 and CO yields

Table 4
Equilibrium and blank reactor (quartz sand) product yields, and carbon balance for the CPOX of TD at O/C = 1.2, P = 0.23 MPa, 900 °C and 50,000 scc/g_{cat}/h [22].

	Equilibrium[a]	Quartz sand (blank)
H_2 yield (%)	90.0	17.0
CO yield (%)	92.0	42.0
CO_2 yield (%)	8.5	17.0
CH_4 yield (%)	0.1	8.0
Ethane yield (%)	0.0	0.7
Ethylene yield (%)	0.0	16.3
Propylene yield (%)	0.0	1.5
C_4-ene yield (%)	0.0	1.0
Benzene yield (%)	0.0	3.9
Carbon balance (%)	100	90

[a] Equilibrium calculations were made using a Gibb's minimization technique in HSC Chemistry Thermodynamic Software [36]. Calculations were made assuming a mixture of 2 mol% TD, 18 mol% O_2, and 80 mol% N_2.

are predicted by equilibrium at an H_2/CO ratio of roughly 1, while olefins and elemental carbon are not predicted by thermodynamics. In the absence of a catalyst (quartz sand), the H_2 and CO yields are produced at levels well below equilibrium, and at an H_2/CO ratio much less than 1. Although quartz shows to be active for CPOX, i.e. converts TD into various gaseous hydrocarbon products as well as some H_2 and CO, its lack of catalytic properties are evident by the poor selectivity towards synthesis gas. In earlier tests (not shown) other materials were examined as diluents (Al_2O_3, and SiC), in addition to the quartz. Results from these studies showed that the reaction temperature was sufficiently high to activate the catalytic properties (albeit low) for each material. The observed activity was similar for each material, as all 3 diluents had a similar product distribution during CPOX of n-tetradecane for 5 h at an O/C = 1.2, GHSV = 50,000 h^{-1}, and 900 °C. The gas compositions produced by these materials, and shown in Table 4 for quartz, therefore represents the lowest or worst product distribution obtainable for a material considered to be inert at these conditions.

3.4.2. CPOX of n-tetradecane

Dry gas product yields (H_2, CO, CO_2 and CH_4) formed as a function of time on stream are shown in Fig. 4 for each catalyst. Olefin yields are presented in Fig. 5. Throughout the course of the initial 1 h reforming step of TD only, high H_2 and CO yields are produced over each catalyst, at values comparable to those predicted by equilibrium (Table 4). Substitution of Ni into either the hexaaluminate or pyrochlore lattice does not appear to alter the catalytic properties of the metal, as both BNHA and LSZN have comparable activity to the 3 wt% Ni/Al_2O_3 catalyst.

3.4.3. Addition of 5 wt% MN and 50 ppmw DBT

After preliminary activity baseline screening with TD only, 5 wt% MN and 50 ppmw DBT are added to the feed. From Figs. 4 and 5 it can be seen that the MN and DBT quickly produces an immediate drop in synthesis gas yields from the equilibrium values for each catalyst.

The loss of activity for the Ni/Al_2O_3 is not surprising, considering the amount of available Ni at the surface that can be readily poisoned by the MN and DBT, as seen by the TPR. Active Ni sites in the BNHA are also easily deactivated, indicating that reducing the critical ensemble number of Ni atoms did not prevent deactivation by MN and DBT. Deactivation occurs more rapidly than the Ni/Al_2O_3, likely because Ni-substituted hexaaluminates are known to have a small number of active sites [4]. The high throughput of contaminants with the apparent strong adsorption tendencies of the contaminants to the surface combines to deactivate these catalysts rapidly. However, it has been found that BNHA catalyst particles can resist deactivation if they are dispersed onto an oxygen-ion conducting oxide [37]. Smith et al. [37] showed that BNHA catalysts with same composition used here, only supported on zirconia doped ceria (ZDC) had stable activity in the presence of MN and DBT during CPOX at 900 °C, while the unsubstituted bulk oxide was deactivated under the same conditions.

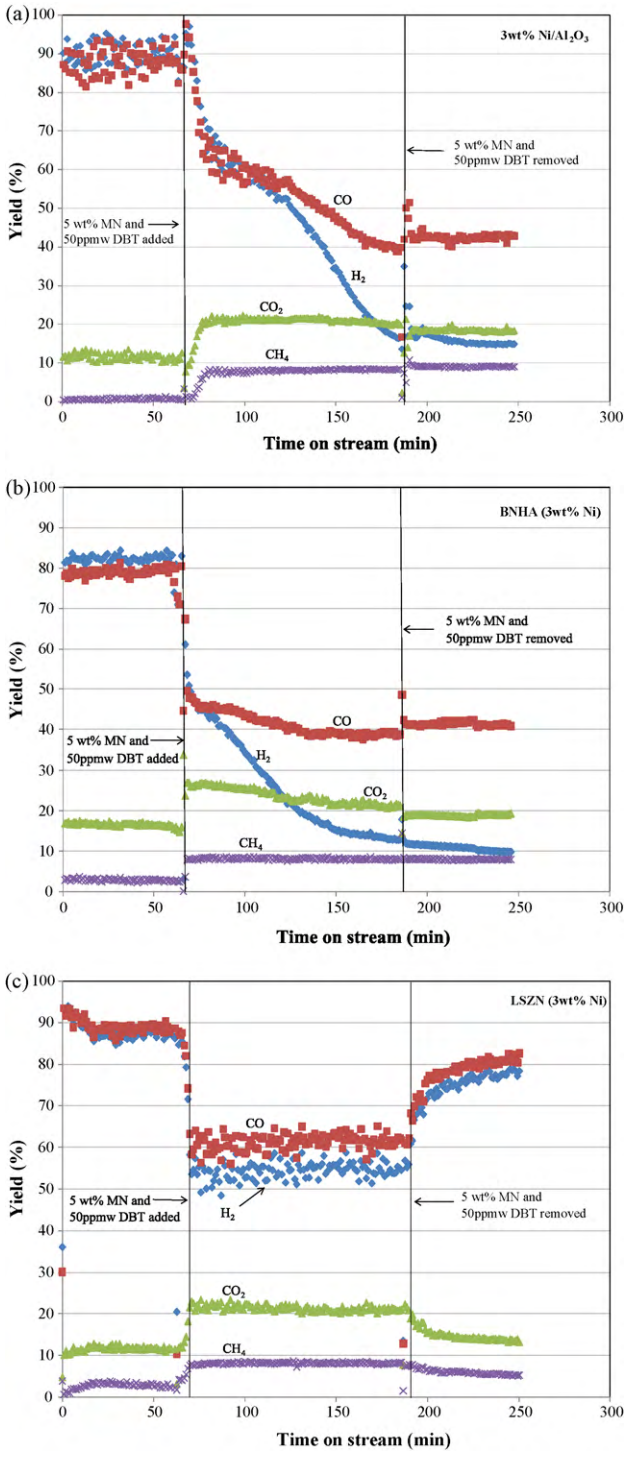

Fig. 4. Dry gas yields for (a) 3 wt% Ni/Al_2O_3, (b) BNHA, and (c) LSZN catalysts during 4 h CPOX of 5 wt% MN and 50 ppmw DBT experiment conducted at O/C = 1.2, 0.23 MPa, 900 °C and 50,000 scc/g_{cat}/h. H2 (♦), CO (■), CO_2 (▲), CH4 (x).

Trends observed for the H_2 and CO yields of both the Ni/Al_2O_3 and BNHA catalysts are consistent with those of Ru/γ-Al_2O_3 [21], Pt/γ-Al_2O_3 and $Co_{0.4}Mo_{0.6}C_x$ [38] catalysts at similar conditions and contaminant levels. Deactivation seen here can be explained by the adsorption of the MN and DBT to the sites responsible for

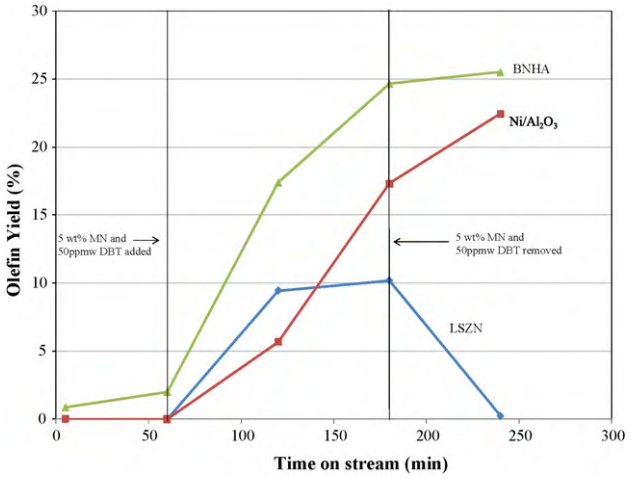

Fig. 5. Olefin yields for 3 wt% Ni/Al_2O_3, BNHA, and LSZN during 4 h CPOX of 5 wt% MN and 50 ppmw DBT experiment at O/C = 1.2, 0.23 MPa, 900 °C and 50,000 scc/g_{cat}/h. Ni/Al_2O_3 (■), BNHA (▲), LSZN (♦).

the predominant H_2 and CO forming reactions, which are located downstream of the initial oxidation zone [38]. Such reactions include steam/CO_2 reforming of hydrocarbon fragments, as well as water gas shift (WGS) and methanation.

The continuous decline in H_2 yields coupled with a commensurate increase in olefins indicates that the steam reforming reaction is responsible for a large portion of H_2 formation, which is consistent with a spatial profile experiment conducted during the CPOX of n-octane by Panuccio and Schmidt [39]. A study by Rabe et al. [40] measured the reformate gas composition as a function of reactor length, and observed the progressive deactivation of a Rh catalyst by sulfur during the autothermal reforming (ATR) of gasoline (containing 6 ppmw sulfur). During the course of their study, they observed a decrease in H_2 and CO products, as well as gasoline and steam conversion over the 3.5 h time on stream. Over this same time, CO_2, CH_4, and hydrocarbon fragments increased. While a direct comparison to the yields in this study cannot be made due to the different catalysts, higher levels of contaminants used in this study, and overall reaction conditions, the general trends of deactivation observed in their study are likely similar to those for the Ni/Al_2O_3 and BNHA catalysts.

The LSZN catalyst is distinguished from the other two by the behavior of its H_2 and CO yields in the presence of the contaminants. Ni substituted into the pyrochlore structure is not continuously deactivated by the MN and DBT, but rather is able to remain active and selective towards H_2 and CO, albeit at lower than precontaminant levels. A noticeable difference is also seen in the behavior of the olefins produced by the LSZN catalyst. The olefin formation rate increases sharply after the first hour in the presence of MN and DBT, but only continues to increase slightly after the initial spike. Together, these results coupled with the behavior of the synthesis gas yields show that the sites involved in the eventual formation of H_2 and CO do not become completely deactivated by the contaminants. Instead, the data would appear to suggest that the adsorption of MN and DBT only decreases the turnover frequency of the active sites, limiting the approach to equilibrium, rather than continuously accumulating on the surface and leading to eventual deactivation.

The Ni in the pyrochlore structure is believed to be able to retain catalytic properties in the presence of the contaminants through improved oxygen-ion conductivity that occurs as a result of Sr substitution [22]. Improving this property provides a localized oxygen source from the pyrochlore lattice to react with the strongly adsorbed carbon forming precursors. Deactivation of the Ni is then prevented during the time scale of this study because the accumulation of refractory surface carbon species is limited. Instead, most surface carbon is gasified into CO/CO_2, and active sites become freed for further reactions.

Table 5
Carbon emitted as CO_2 during TPO.

Catalyst	Amount of carbon ($g_{carbon}/g_{catalyst}$)
Ni/Al_2O_3	2.0
BNHA	2.4
LSZN	0.4

3.4.4. CPOX of n-TD during recovery period

After the contaminants are removed from the feed, activity does not return for the Ni/Al_2O_3 and BNHA catalysts. Evaluating the gaseous product yields during the recovery period to those produced in the absence of a catalyst (Table 4) shows comparable product selectivity. High selectivity to olefins is observed, and H_2 and CO yields are produced at an H_2/CO ratio of much less than 1. This indicates both catalysts have been irreversibly deactivated by the contaminants. Meanwhile, the LSZN is able to recover a portion of its initial activity, showing that most of the effects of the MN and DBT are reversible. H_2 and CO yields both increase, while olefin products return to precontaminant levels, and CO_2 and CH_4 yields both decrease. The ability to recover activity suggests that the contaminants act, for the most part, as kinetic inhibitors to the H_2 and CO producing sites. However, total initial activity is not recovered, signifying some activity loss was irreversible.

3.5. Temperature programmed oxidation (TPO)

Table 5 presents the amount of carbon formed on each catalyst during the reforming studies. From these numbers a strong correlation between catalyst activity and carbon formation is observed. Deactivation of Ni/Al_2O_3 and BNHA appears to be associated with carbon accumulation on the active sites. Both catalysts show an irreversible loss in activity once the contaminants are removed from the feed, and both have roughly similar amounts of oxidizable carbon. Owing to its oxygen-ion conducting properties, the Ni pyrochlore (LSZN) has the least amount of carbon deposited on the surface. The carbon that does deposit appears to do so more indiscriminately on the surface of the LSZN, rather than just the active sites, as the catalyst is able to recover a much its initial activity (Fig. 4c).

TPO profiles indicate the reactive nature of the carbon (Fig. 6). The Ni/Al_2O_3 has a slight low temperature shoulder at ~588 °C, which is overlapped by a main peak centered at 650 °C, indicating two types of carbon on the surface. The low temperature shoulder can likely be assigned to carbon formed on/near the surface Ni-species. This may be a form of amorphous carbon on/near the metal that forms during the reforming of hydrocarbons over Ni catalysts [41]. Carbon oxidized in the region of the main peak is likely to be filamentous in nature. Two separate studies [42,43] noted a similarly shaped peak over a similar temperature range during their respective TPO of a Ni/Al_2O_3 catalyst used for steam reforming of propane.

TPO curves for BNHA and LSZN qualitatively illustrate the difference in carbon formation on the two Ni-substituted catalysts. However, despite the differences in amount, the deposited carbon appears to be similar in reactivity for the two catalysts as it is oxidized over a similar temperature range. Although this temperature range overlaps with the suspected filamentous carbon on the Ni/Al_2O_3, it is unlikely that either of these catalysts contains any filamentous carbon. As confirmed by XANES, Ni was determined to occupy coordinated environments consistent with substitution

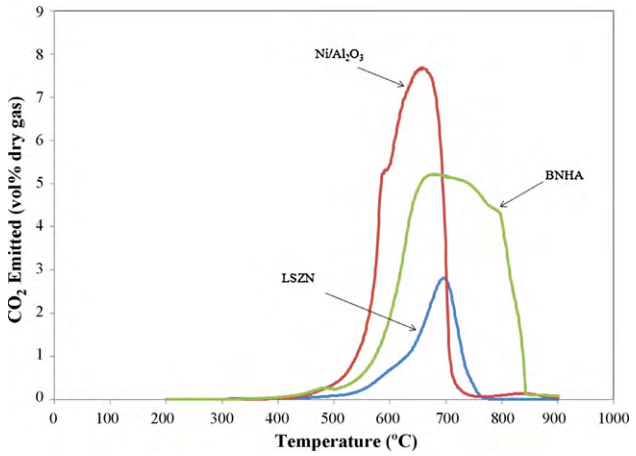

Fig. 6. TPO profiles for Ni/Al_2O_3, BNHA, and LSZN catalysts after 4 h CPOX of 5 wt% MN and 50 ppmw DBT experiment conducted at O/C = 1.2, 0.23 MPa, 900 °C and 50,000 scc/g_{cat}/h.

into the hexaaluminate and pyrochlore structures, respectively. In such a coordination, dispersed Ni atoms at the surface are unlikely to be able to form filamentous carbon because they lack sufficiently sized Ni particles for carbon to diffuse through to initiate filament growth [12]. However, the carbon which does accumulate on both the BNHA and LSZN is likely a form of pyrolytic encapsulating carbon [15]. Given the reaction temperature and chemical structure of the contaminants (mainly MN), this carbon probably has some polyaromatic character [44]. Higher temperatures are required to oxidize this type of carbon not only because of its refractory nature, but also because there is less Ni at the surface to help gasify the carbon.

4. Conclusions

Ba–Ni-substituted hexaaluminate (BNHA) and Ni-Sr substituted lanthanum zirconate pyrochlore (LSZN) catalysts (3 wt% Ni each) were compared to a supported 3 wt% Ni/Al_2O_3 catalyst for the catalytic partial oxidation of a surrogate fuel mixture into synthesis gas. XRD patterns revealed a single phase $BaAl_{12}O_{19}$ was obtained for the hexaaluminate, while the pyrochlore phase formed along with a defect $SrZrO_3$ perovskite for the LSZN. TPR results showed Ni atoms were accessible in all three catalysts and were reducible. Features from XANES spectra are consistent with Ni-metal being substituted into the hexaaluminate and pyrochlore structures, as spectra for each catalyst showed different coordination environments for Ni compared to a NiO standard. During CPOX reaction studies, Ni/Al_2O_3 and BNHA catalysts were irreversibly deactivated during the 2 h in which the contaminants were present, while LSZN was only kinetically inhibited. Activity loss was strongly linked to carbon formation. Activity loss of both Ni/Al_2O_3 and BNHA was observed to be irreversible once the contaminants were removed from the feed, and both had roughly similar amounts of carbon on the surface. LSZN catalyst had least amount of carbon deposited, and recovered a significant portion of its initial activity return during the 1 h recovery period. The resistance to carbon formation by the pyrochlore may be attributed to the oxygen-ion conductivity properties of the Sr-containing pyrochlores.

Acknowledgements

This work was performed in support of the National Energy Technology Laboratory's on-going research in fuel processing, under contract # DE-AC26-04NT41817 subtask 41817.610.01.01. The authors would also like to gratefully acknowledge Donald Floyd for his invaluable contributions to this work in performing the experiments.

References

[1] S. Pengpanich, V. Meeyoo, T. Rirksomboon, J. Schwank, Appl. Catal. A 302 (2006) 133.
[2] T. Utaka, S.A. Al-Drees, J. Ueda, Y. Iwasa, T. Takeguchi, R. Kikuchi, K. Eguchi, Appl. Catal. A 247 (2003) 125.
[3] J. Zhang, Y. Wang, R. Ma, D. Wu, Appl. Catal. A 243 (2003) 251.
[4] T.H. Gardner, D. Shekhawat, D.A. Berry, M.W. Smith, M. Salazar, E.L. Kugler, Appl. Catal. A 323 (2007) 1.
[5] R. Kikuchi, Y. Iwasa, T. Takeguchi, K. Eguchi, Appl. Catal. A 281 (2005) 61.
[6] B.D. Gould, X. Chen, J.W. Schwank, Appl. Catal. A 334 (2008) 277.
[7] X. Chen, B.D. Gould, J.W. Schwank, Appl. Catal. A 356 (2009) 137.
[8] S. Freni, G. Calogero, S. Cavallaro, J. Power Sources 87 (2000) 28.
[9] T. Miyazawa, T. Kimura, J. Nishikawa, S. Kado, K. Kunimori, K. Tomishige, Catal. Today 115 (2006) 254.
[10] N.C. Triantafyllopoulos, S.G. Neophytides, J. Catal. 217 (2003) 324.
[11] D.L. Trimm, Chem. Eng. Process. 18 (1984) 137.
[12] X. Chen, A.R. Tadd, J.W. Schwank, J. Catal. 251 (2007) 374.
[13] C.H. Bartholomew, Appl. Catal. A 212 (2001) 17.
[14] D. Chen, R. Lødeng, A. Anundskås, O. Olsvik, A. Holmen, Chem. Eng. Sci. 56 (2001) 1371.
[15] D.L. Trimm, Catal. Today 49 (1999) 3.
[16] R.G. Tailleur, Catal. Today 130 (2008) 492.
[17] L.F. Brown, Int. J. Hydrogen Energy 26 (2001) 381.
[18] J. Hepola, P. Simell, Appl. Catal. B 14 (1997) 305.
[19] E. Ruckenstein, H.Y. Wang, J. Catal. 205 (2002) 289.
[20] D.J. Haynes, D.A. Berry, D. Shekhawat, J.J. Spivey, Catal. Today 145 (2009) 121.
[21] D.J. Haynes, A. Campos, D.A. Berry, D. Shekhawat, A. Roy, J.J. Spivey, Catal. Today. doi:10.1016/j.cattod.2009.03.025.
[22] D.J. Haynes, D.A. Berry, D. Shekhawat, J.J. Spivey, Catal. Today 136 (2008) 206.
[23] M.P. Pechini, Method of preparing lead and alkaline earth titanates and niobates and coating method using the same to form a capacitor, U.S. Patent 3,330,697 (1963).
[24] D. Shekhawat, T.H. Gardner, D.A. Berry, M. Salazar, D.J. Haynes, J.J. Spivey, Appl. Catal. A 311 (2006) 8.
[25] D. Shekhawat, D.A. Berry, D.J. Haynes, J.J. Spivey, Fuel 88 (2009) 817.
[26] I. Hayakawa, H. Kamizono, J. Nucl. Mater. 202 (1993) 163.
[27] H.H. Ibrahim, P. Kumar, R.O. Idem, Energy Fuels 21 (2007) 570.
[28] H.H. Ibrahim, R.O. Idem, Energy Fuels 22 (2008) 878.
[29] W. Chu, W. Yang, L. Lin, Appl. Catal. A 235 (2002) 39.
[30] F. Yin, S. Ji, P. Wu, F. Zhao, C. Li, J. Mol. Catal. A: Chem. 294 (2008) 27.
[31] S. Li, X. Wang, J. Alloys Compd. 432 (2007) 333.
[32] F. Farges, M. Munoz, R. Siewert, V. Malavergne, G.E. Brown, H. Behrens, M. Nowak, P.E. Petit, Geochim. Cosmochim. Acta 65 (2001) 1679.
[33] H.C. Huang, Y.L. Wei, Y.W. Yang, J.F. Lee, J. Electron. Spectosc. Relat. Phenom. 144 (2005) 825.
[34] J. Iqbal, B.Q. Wang, X.F. Liu, D.P. Yu, B. He, R.H. Yu, New J. Phys. 11 (2009).
[35] F. Farges, G.E. Brown, P.E. Petit, M. Munoz, Geochim. Cosmochim. Acta 65 (2001) 1665.
[36] A. Roine, HSC Chemistry 6.12 ed., Outotec Research Oy, 2007.
[37] M.W. Smith, D.A. Berry, D. Shekhawat, D.J. Haynes, J.J. Spivey, Fuel. doi:10.1016/j.fuel.2009.12.017.
[38] D.J. Haynes, D.A. Berry, D. Shekhawat, T.-C. Xiao, M.L.H. Green, J.J. Spivey, Ind. Eng. Chem. Res. 47 (2008) 7663.
[39] G.J. Panuccio, L.D. Schmidt, Appl. Catal. A 332 (2007) 171.
[40] S. Rabe, F. Vogel, T.-B. Truong, T. Shimazu, T. Wakasugi, H. Aoki, H. Sobukawa, Int. J. Hydrogen Energy 34 (2009) 8023.
[41] X. Zhu, P. Huo, Y.-P. Zhang, D.-G. Cheng, C.-J. Liu, Appl. Catal. B 81 (2008) 132.
[42] L. Zhang, X. Wang, B. Tan, U.S. Ozkan, J. Mol. Catal. A: Chem. 297 (2009) 26.
[43] S. Natesakhawat, R.B. Watson, X. Wang, U.S. Ozkan, J. Catal. 234 (2005) 496.
[44] M. Guisnet, P. Magnoux, Appl. Catal. A 212 (2001) 83.